

Corrosion Inhibition Activity and Adsorption behavior of 3-Amino-1, 2, 4-Triazole on copper

Yunxiao Wan, Zhenlan Qin, Qunjie Xu*, Mojing Chen, YuLin Min, Meiming Li

Shanghai Key Laboratory of Materials Protection and Advanced Materials in Electric Power, Shanghai Engineering Research Center of Energy-Saving in Heat Exchange Systems, Shanghai University of Electric Power, 2588 Changyang Road, Yangpu District, Shanghai 200090, China

*E-mail: xuqunjie@shiep.edu.cn

Received: 28 July 2017 / Accepted: 16 September 2017 / Published: 12 October 2017

In this paper, a borax media was introduced to improve inhibition effect of 3-amino-1, 2, 4-triazole (ATA) towards the corrosion of copper in basic solution. Results showed that the inhibition efficiency is enhanced to 97.65% significantly at an ATA concentration of $30 \text{ mg}\cdot\text{L}^{-1}$. The correlation analysis of electrochemical and photoelectrochemical properties indicated that the ATA is a great corrosion inhibitor for copper in the borax buffer solution. Surface enhanced Raman scattering (SERS) spectroscopy revealed that the inhibition of copper corrosion is mainly due to enhancing adsorption of ATA molecules on the surface of copper. The typical of chemisorptions was found to obey Langmuir's adsorption isotherm, which is consistent with the quantum calculation.

Keywords: Copper; Photoelectrochemistry; SERS; Corrosion; Inhibitor

1. INTRODUCTION

Copper is widely used in industrial applications because of its high electrical and thermal conductivities, good mechanical workability and relatively noble properties. However, copper may easily suffer from corrosion in sea water, acid media or alkaline solutions. Thus much attention has been paid to improve the effect of copper against corrosion in aggressive media [1-3]. Employment of organic inhibitors is one of promising strategies to control the corrosion of copper. Meanwhile, benzotriazole (BTA) and its derivatives are the traditional inhibitors for copper in recent 50 years [4-7]. However, the high toxicity leads to seriously environmental destruction, limiting their practical application. Therefore, extensive studies have been performed to develop environmentally friendly alternatives [8-10]. Triazole-type compounds are environmentally acceptable and good corrosion

inhibitors in HCl solutions [11-13]. Among the triazole derivatives, 3-amino-1, 2, 4-triazole (ATA, Fig. 1) is one of attractive candidates due to high efficiency for against corrosion of copper in aerated synthetic sea water [14] or acid media [15-17]. However, the maximum of inhibition efficiency only reached to 96% as far as we known. And to the best of our knowledge, less attention has been paid so far towards investigating ATA as the inhibitor for copper in alkaline solutions.

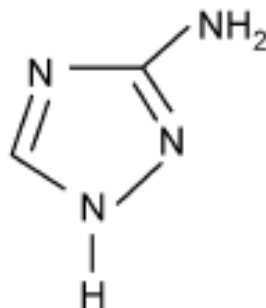


Figure 1. The structure of 3-Amino-1, 2, 4-triazole (ATA)

Generally, the effectiveness of the inhibitor to provide corrosion protection relies upon the interaction between the inhibitor and the metal surface. The properties of the surface of the metal, the adsorption mode, the chemical structure of the inhibitor and the type of the electrolyte solution may play crucial effects on the interaction between inhibitor and the metal surface [18]. Electrochemical and photoelectrochemical methods have been employed to elucidate the inhibition efficiency and mechanism; the latter especially since it is regarded as an in-situ technique and can supply some important information, which cannot be obtained by conventional electrochemical methods and surface analysis techniques [19-26].

Herein, we reported on high inhibition effect for copper corrosion by ATA inhibitor in a borax media (pH=9.2), which was demonstrated by using a series of joint techniques, including cyclic voltammetry, photoelectrochemical and electrochemical impedance analysis. Additionally, surface enhanced Raman scattering spectroscopy (SERS) is also employed to confirm the nature and orientation of the species adsorbed on the copper surface.

2. EXPERIMENTAL

2.1 Chemicals and electrode treatment

ATA and other reagents were used as received. The copper electrode was polished successively with different grades (3[#]-6[#]) of emery papers, washed with deionized water, degreased with acetone, and finally rinsed with deionized water. The electrolyte was a borax buffer solution, which consisted of 0.075mol/L Na₂B₄O₇ and 0.150mol/L H₃BO₃ and its pH maintained at pH=9.2. Then, ATA was added

to the borax buffer solution to prepare a mixed solution in which the concentrations of ATA were $0 \text{ mg}\cdot\text{L}^{-1}$, $20 \text{ mg}\cdot\text{L}^{-1}$, $30 \text{ mg}\cdot\text{L}^{-1}$ and $40 \text{ mg}\cdot\text{L}^{-1}$, respectively.

2.2 Electrochemical and photoelectrochemical measurements

Photoelectrochemical measurements were provided by a PARC M273 potentiostat (EG&G), a PARC 5208EC lock-in analyzer, a 1000 W Xe lamp, a WDG-1A monochromator (Siping Optical Instruments), an ND-4chopper (Nanjing University of China), and a LM20A-200 X-Y recorder. For spectral measurements, the light intensity was measured by a calibrated silicon photodiode, and the light flux never exceeded $20 \text{ mW}\cdot\text{cm}^{-2}$. The wavelength of mono-chromate light was 420 nm. The modulation frequency of chopper was 39 Hz. A homemade three-electrode cell with an end of quartz window was used. The reference electrode was a saturated calomel electrode (SCE), whereas the counter electrode was a Pt electrode. The surface area of the working electrode was 0.24 cm^2 .

Electrochemical measurements were performed in a PARC M273 potentiostat (EG&G) with a PARC1025 frequency analyzer. The electrochemical impedance spectroscopy (EIS) experiments were performed at open circuit potential over a frequency range of 100 kHz to 50 mHz. The sinusoidal potential perturbation was 5 mV in amplitude. The potentiodynamic scan rate was 2 mV/s .

2.3 Raman spectroscopy experiments

The Raman spectra were measured with LabRam I type (Dilor, France) Raman spectrometer using the 632.8 nm line as the excitation beam. Copper electrodes were immersed in borax buffer solution (concentration of ATA is $30 \text{ mg}\cdot\text{L}^{-1}$) solution at different voltages for 30 min. Then, surface enhanced Raman spectroscopy (SERS) tests were performed on the ATA adsorbed on copper.

3. RESULTS AND DISCUSSION

3.1 Photoelectrochemical measurements

Fig. 2 shows the current density vs. potential ($i-\phi$) and photocurrent density vs. potential ($i_{\text{ph}}-\phi$) characteristics observed on a Cu electrode in a borax buffer solution (pH=9.2) at various concentrations of ATA, respectively. The anodic peak A I corresponds to the oxidation of Cu (0) to Cu (I) on the electrode surface, indicating the formation of Cu_2O film and the anodic dissolution of Cu through Cu_2O film [26]. The anodic peak A II corresponds to the further oxidation of Cu (I) to Cu (II). The cathodic peaks C1 and C2 correspond to the reduction of Cu (II) to Cu (I) and Cu (I) to Cu (0), respectively [27]. CuO is a narrow bandgap semiconductor with $E_g = 0.60 \text{ eV}$. A photocurrent has not been observed from CuO on the Cu electrode because of its low resistivity and high recombination rate. On the negative potential scan, i_{ph} gradually increases as CuO is reduced to Cu_2O , the value of i_{ph} reaches the maximum at -0.55 V(SCE) and decreases after -0.55 V(SCE) as Cu_2O is gradually reduced to Cu. When potentials are lower than -0.58 V(SCE) , i_{ph} is found close to zero as the reduction of

Cu_2O is almost complete, and the electrode surface is nearly reduced to the metallic state. The potential corresponding to the cathodic photocurrent $i_{\text{ph}} = 0$ is defined as ϕ_v . The ϕ_v of curve 1 in Fig. 2b is -0.92 V(SCE) . Curve 2 in Fig. 2a and 2b shows that the cathodic i_{ph} vs. potential containing $5 \text{ mg}\cdot\text{L}^{-1}$ ATA is different from that absence of ATA; cathodic $i_{\text{ph, max}}$ is larger than that without the inhibitor. It is generally considered that $i_{\text{ph, max}}$ is caused by the reduction of CuO to Cu_2O on the reverse potential scan, and cathodic i_{ph} increases with the amount of the surface of Cu_2O . Curve 3 in Fig. 2a and 2b shows that on the positive scan anodic peak AI and AII are further reduced at an ATA concentration of $10 \text{ mg}\cdot\text{L}^{-1}$, but the $i_{\text{ph, max}}$ is increased. Anodic peak AI and AII decrease with increasing ATA concentration and close to zero at $20 \text{ mg}\cdot\text{L}^{-1}$, $30 \text{ mg}\cdot\text{L}^{-1}$, $40 \text{ mg}\cdot\text{L}^{-1}$, respectively.

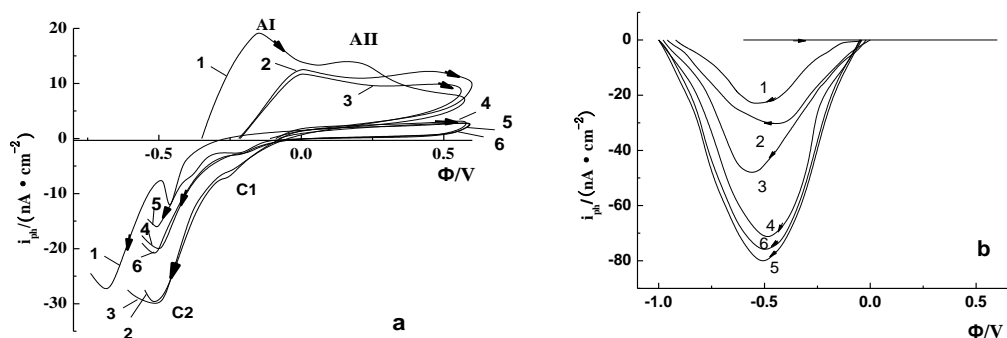


Figure 2. i - ϕ (a) and i_{ph} - ϕ (b) curves for copper electrode in borax buffer solution with different concentrations of ATA. Scan rate: 1 mV/s ; modulation frequency: 39 Hz ; irradiation wavelength: 420 nm ; $C_{\text{ATA}}/(\text{mg}\cdot\text{L}^{-1})$: (1) 0, (2) 5, (3) 10, (4) 20, (5)30, (6)40

When the concentration of ATA is $5 \text{ mg}\cdot\text{L}^{-1}$ on the negative potential scan to -0.92 V(SCE) , the cathodic photocurrent still does not reach to zero ($i_{\text{ph}}=-2.4 \text{ nA}\cdot\text{cm}^{-2}$), which suggests that the Cu_2O on the electrode surface does not reduce to Cu . The cathodic photocurrents $|i_{\text{ph}}|$ for a Cu electrode at $5, 10, 20$ and $30 \text{ mg}\cdot\text{L}^{-1}$ ATA are $30.5, 48.5, 71.5,$ and $82 \text{ nA}\cdot\text{cm}^{-2}$, respectively, indicating that the larger the ATA concentration, the higher the value of the cathodic photocurrent. ATA has corrosion inhibition for copper due to the formation of $\text{Cu/Cu}_2\text{O/Cu(I)ATA}$ film on the copper surface. Cu(I)ATA film combine strongly with the Cu_2O layer, which stabilizes the Cu_2O film on the surface. The ϕ_v is more negative, and the $|i_{\text{ph}}|$ will be larger, and therefore the ATA inhibition cloud be shown better effects. Consequently, the effectiveness of the copper corrosion inhibitors could be evaluated by the ϕ_v and the $|i_{\text{ph}}|$. It is shown from Fig. 2 that the value of the cathodic photocurrent at ATA $40 \text{ mg}\cdot\text{L}^{-1}$ is smaller than that at ATA $30 \text{ mg}\cdot\text{L}^{-1}$, but larger than the absence of ATA, indicating that ATA at this concentration still exhibits the corrosion inhibition. The results show that the best concentration of ATA is $30 \text{ mg}\cdot\text{L}^{-1}$ in this study.

3.2 Electrochemical measurements

The EIS data are presented in Nyquist plots. Fig. 3 gives the typical Nyquist plots for copper electrode in the borax buffer solution after 30 min immersion with different concentrations of ATA.

The Nyquist plots are all semicircular and the chord is the symbol of the corrosion resistance (R_f), the larger the R_f , the better the inhibition effect [28-32]. Compared with the electrode without ATA, the electrodes at various concentrations of ATA have longer chords, the higher R_f , indicating that ATA at various concentration has obvious corrosion inhibition for copper. When increasing the concentration of ATA from 0 to 30 $\text{mg}\cdot\text{L}^{-1}$, the R_f keeps increasing and reaches the maximum at 30 $\text{mg}\cdot\text{L}^{-1}$ of ATA. However, when the concentration of ATA exceeds 30 $\text{mg}\cdot\text{L}^{-1}$, the corresponding chord decreases. So the optimum concentration of ATA is 30 $\text{mg}\cdot\text{L}^{-1}$, which reinforces the result from the photoelectrochemical measurements.

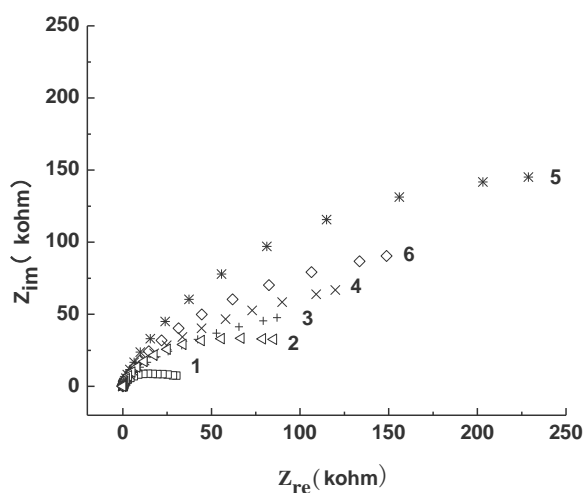


Figure 3. Nyquist plots for copper in borax buffer solution (pH=9.2) with different concentrations of ATA. $C_{ATA}/(\text{mg}\cdot\text{L}^{-1})$: (1) 0, (2) 5, (3) 10, (4) 20, (5)30, (6)40

Fig.4 shows the potentiodynamic polarization curve plots for copper in the borax buffer solution (pH=9.2) with different concentrations of ATA. The parameters, such as corrosion potential (E_{corr}), corrosion current (i_{corr}) and the inhibition efficiency (η), are listed in Table1. The η applied to evaluate the inhibition effects of ATA for copper corrosion was calculated according to Eq. (1):

$$\eta = \left(I_{\text{corr}}^0 - I_{\text{corr}} \right) / I_{\text{corr}}^0 \quad (1)$$

I_{corr}^0 and I_{corr} are the corrosion current densities in the absence and presence of ATA, respectively. It is clear that the corrosion potential shifts to the noble direction in the presence of different concentrations of ATA, indicating that ATA may inhibit the anodic reaction and keeps metal in a more stable state. Meanwhile, the i_{corr} decreases with the increasing of ATA concentrations. Compared to the bare copper electrode, the i_{corr} reaches the minimum value when adding to 30 $\text{mg}\cdot\text{L}^{-1}$ of ATA and its η is the maximum value of 97.65%, with is far greater than the maximum of 96% of the other as far as we known. This further confirms the conclusion obtained by the photoelectrochemical measurements and EIS that ATA can act as a powerful inhibitor against corrosion of copper in alkaline solutions.

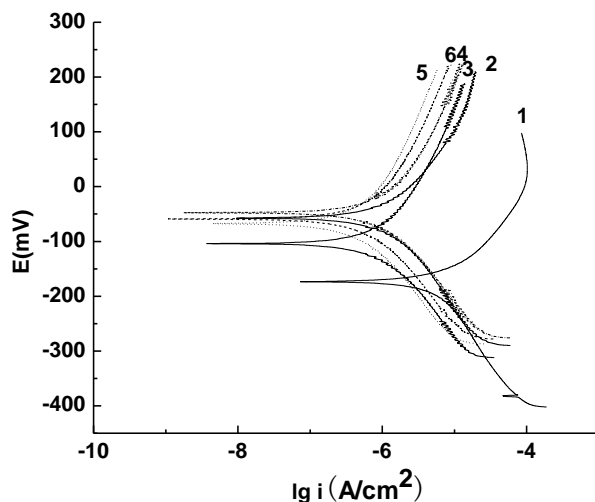


Figure 4. Potentiodynamic polarization curve plots for copper in borax buffer solution (pH=9.2) with different concentrations of ATA. $C_{ATA}/(\text{mg}\cdot\text{L}^{-1})$: (1) 0, (2) 5, (3) 10, (4) 20, (5)30, (6)40

Table 1. Electrochemical parameters of the copper electrodes in borax buffer solution without and with difference concentrations of ATA.

$C(\text{mg}\cdot\text{L}^{-1})$	$E_{\text{corr}}(\text{V})$	$I_{\text{corr}}(\mu\text{A}\cdot\text{cm}^{-2})$	$\eta(\%)$
0	-0.1736	8.075	/
5	-0.05736	1.215	84.96
10	-0.104	1.208	85.04
20	-0.04769	1.008	87.52
30	-0.06782	0.7502	97.65
40	-0.05954	0.9546	88.18

3.3 Adsorption behavior

To study the adsorption behavior of ATA on copper surface, the inhibition efficiency (η) obtained from the polarization curves at 25°C were represented as the surface coverage degree (θ) to fit the Temkin, Langmuir, and Frumkin adsorption isotherm [33-35]. The results show that Langmuir adsorption isotherm is closest to the description of the adsorption behavior of the studied inhibitor. The Langmuir adsorption isotherm is given by Equation (2):

$$\frac{C}{\theta} = \frac{1}{K} + C \quad (2)$$

Where C is the inhibitor concentration in the electrolyte ($\text{mol}\cdot\text{L}^{-1}$), K is the adsorption equilibrium constant, θ is the surface coverage degree. The plot of C/θ against C gives a straight line as shown in Fig. 5. It is found that the linear correlation coefficient R is 0.99952 and the slope is 1.1126. This isotherm is found to fit well with the Langmuir type, suggesting that each ATA molecule occupies about 1.1 adsorption sites on the copper surface and it is mono-molecule layer adsorption.

The adsorption equilibrium constant K is $1.9920 \times 10^5 \text{ L} \cdot \text{mol}^{-1}$. K is related to the free energy of adsorption, ΔG^0 , with Equation [36] (3):

$$K = \frac{1}{55.5} \exp\left(\frac{-\Delta G^0}{RT}\right) \quad (3)$$

The value of $55.5 \text{ mol} \cdot \text{L}^{-1}$ in the above equation is the concentration of $1 \text{ mol} \cdot \text{L}^{-1} \text{ H}_2\text{O}$ in solution. The free energy of adsorption (ΔG^0), can be calculated to be $-40.19 \text{ kJ} \cdot \text{mol}^{-1}$ in the case of ATA. The negative values of ΔG^0 ensure the spontaneity of the adsorption process. Generally, values of ΔG^0 around $-20 \text{ kJ} \cdot \text{mol}^{-1}$ or lower are consistent with the electrostatic interaction (physisorption); those about $-40 \text{ kJ} \cdot \text{mol}^{-1}$ or higher involve charge sharing or a transfer from the inhibitor molecules to the metal surface to form a co-ordinate type of bond (chemisorption) [37, 38]. For the adsorption of ATA on Cu, the calculated value of slightly under $-40 \text{ kJ} \cdot \text{mol}^{-1}$ shows that the adsorption is of a typical chemical adsorption.

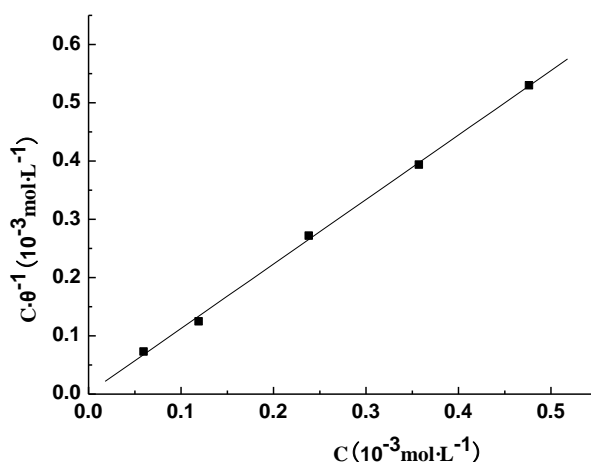


Figure 5. Curve fitting of the corrosion data for copper electrode according to Langmuir thermodynamic kinetic

3.4 Raman spectroscopy investigations

Surface enhanced Raman spectroscopy (SERS) is a powerful tool in analyzing metal adsorbate bonding and in elucidating of the surface orientation of adsorbed molecules [39, 40]. SERS is used in order to gain more information about the inhibition mechanism of ATA for copper corrosion. Fig. 6 and 7 show the Raman spectrum of solid ATA and SERS spectrum of ATA adsorbed onto copper at open circuit potential (-0.21 V), respectively. The SERS spectra of $0.24 \text{ mg} \cdot \text{L}^{-1}$ of ATA on copper at the potential range of -1.0 to 1.0 are displayed in Fig. 8. The assignment of the peaks is listed in Table 2. As shown in Fig. 6, the peaks at 741 , 1053 , 1216 and 1287 cm^{-1} at open circuit potential are assigned to the ring breathing mode, in-plane ring stretching vibration mode, $-N-H$ deformation vibration mode and $-C-H$ in-plane stretching vibration mode, respectively. Compared with the Raman spectra of solid ATA, all the peaks mentioned above have shifted at varying degrees. The peaks at 748 ,

1048, 1074, 1218 and 1291 cm^{-1} in the Raman spectra of solid ATA are assigned to the ring breathing mode, in-plane ring stretching vibration mode, -N-N vibration mode, -N-H deformation vibration mode and -C-H in-plane stretching vibration mode, respectively. It is clear from Fig. 8 that the peaks and the intensity of Raman signals are different with the adsorption of ATA at different potentials. The intensities of Raman signals reach the maximum when the potential is -0.6V and some corresponding Raman parameters are listed in Table 2. SERS reveals that the inhibition of ATA for copper corrosion caused the adsorption of ATA molecules on the surface, the formation of a complex with Cu^+ and prevention of the occurrence of copper chloride complexes, CuCl_2 . The present findings are compatible with the results in the case of ATA as the inhibitor in sea water solutions [14], or acid media [16].

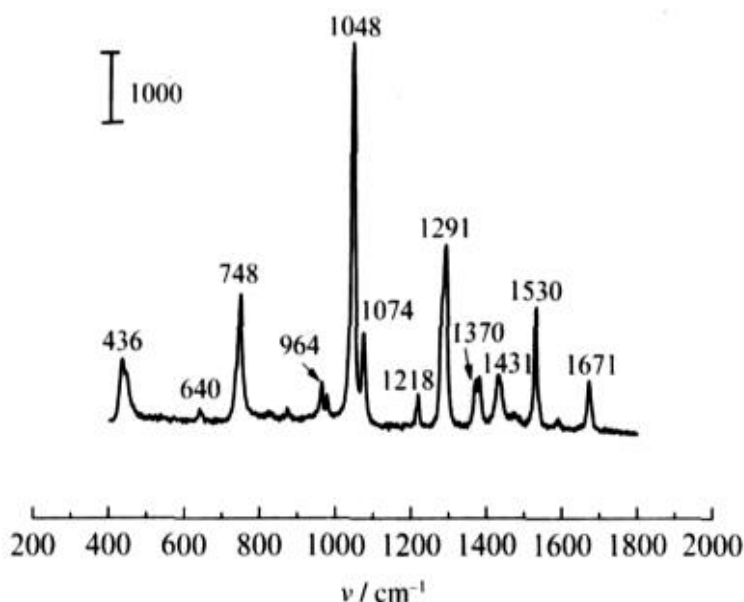


Figure 6. Raman spectrum of solid ATA

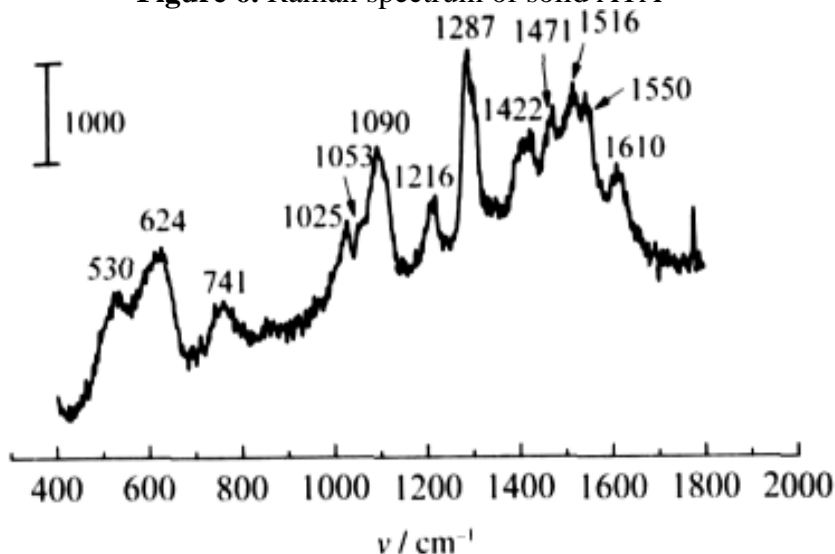
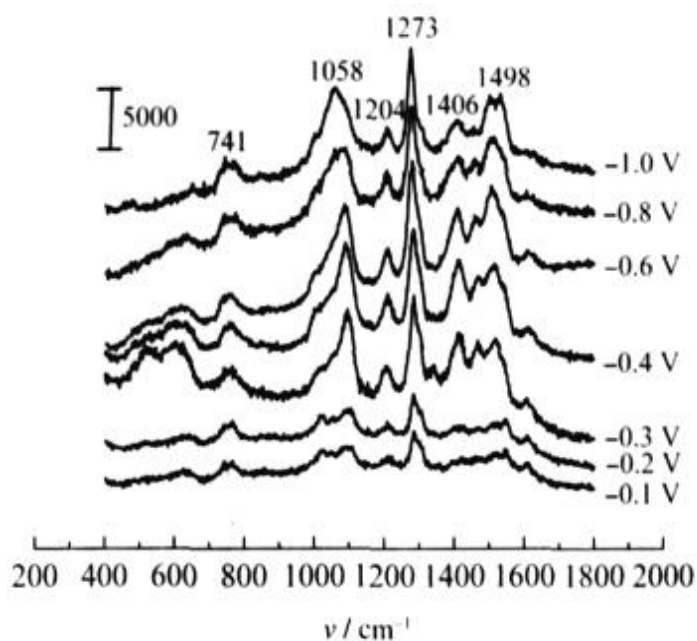


Figure 7. SERS spectrum of ATA adsorbed onto copper at open circuit potential (-0.21 V)

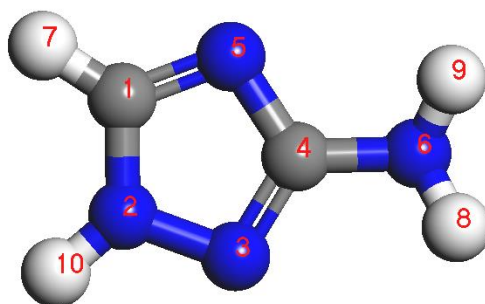
Table 2. Assignment of Raman spectrum of solid ATA and SERS of ATA on Cu in borax buffer solution

Solid ATA	Assignment	E / V	
		-0.21*	-0.6
748(s)	triazole ring breathing	741 (w)	752 (w)
1048(vs)	in plane triazole ring stretching	1053 (w)	-
1074(m)	-N-N- stretching	-	1080(m)
1218(w)	-NH- deformation	1216 (w)	1209(w)
1291(s)	-CH in plane bending	1287(vs)	1286 (s)

* Open circuit potential

**Figure 8.** SERS spectra of $0.24 \text{ mmol}\cdot\text{L}^{-1}$ ATA on copper at different potentials

3.5 Quantum calculations of ATA molecule

**Figure 9.** the structure of the ATA molecule

The structure of the ATA molecule is given in Fig. 9. According to the hybrid orbital theory, the N3 and N5 atoms have sp² hybridization and could provide lone-pair electrons to the empty d-orbital of Cu atom, respectively.

To investigate the reactive sites of the ATA molecule, all total energy density functional theory calculations were carried out using Dmol3 module on the fine level. The exchange correlation functional utilized was GGA-PBE [41]. The Fukui indices were listed in table 3. The higher value of f⁺ means greater nucleophilic ability while higher value of f⁻ represents greater electrophilic ability [42]. The calculation results show that the N3 atom has a higher value of f⁺, which means a greater nucleophilic ability. Meanwhile, it might be the suitable adsorption site.

Table 3. the Fukui indices of the ATA molecule

Atom	f ⁺	f ⁻
C1	0.225	0.077
N2	0.079	0.058
N3	0.164	0.175
C4	0.056	0.054
N5	0.120	0.101
N6	0.041	0.202
H7	0.125	0.097
H8	0.057	0.082
H9	0.047	0.083
H10	0.087	0.070

Based on the above calculation, the adsorption model of the vacuum slab on the Cu (100) surface was showed in Fig. 10. The lowest layer of the Cu atoms were fixed. The height of the vacuum slab is 20Å. The calculation results were listed in table 4. The adsorption energies were calculated using the equation (1) [43]:

$$E_{\text{adsorption}} = E_{\text{total}} - E_{\text{molecule}} - E_{\text{surface}} \quad (1)$$

Where $E_{\text{adsorption}}$ is the adsorption energy, E_{molecule} is the total energy of the ATA molecule. E_{surface} is the total energy of the clean Cu (100) slab, and E_{total} is the total energy of the ATA on Cu (100).

Table 4. the adsorption energy of the ATA

$E_{\text{molecular}}$ (Ha)	E_{surface} (Ha)	E_{total} (Ha)	$E_{\text{adsorption}}$ (Ha)
-297.3958	-10681.3268	-10978.7536	-0.0310

Eadsorption is calculated to be -0.0310 Ha, i.e. -81.39KJ/mol. Furthermore, the ATA molecule was adsorbed vertically on the top site of the Cu atom via N3 atom, which could agree to the previous works [44, 45]. For example, Sh.Q. Sun [44] reported that imidazole (IMD) and benzimidazole

(BIMD) molecules were adsorbed perpendicularly on the top site of the Cu atom through a single nitrogen atom. A. Kosari [45] anticipated that ATA would be adsorbed vertically through N3 atoms to the surface by the analysis of electrostatic potential and molecular orbital. Moreover, the simulation result is consistent with the experimental result.

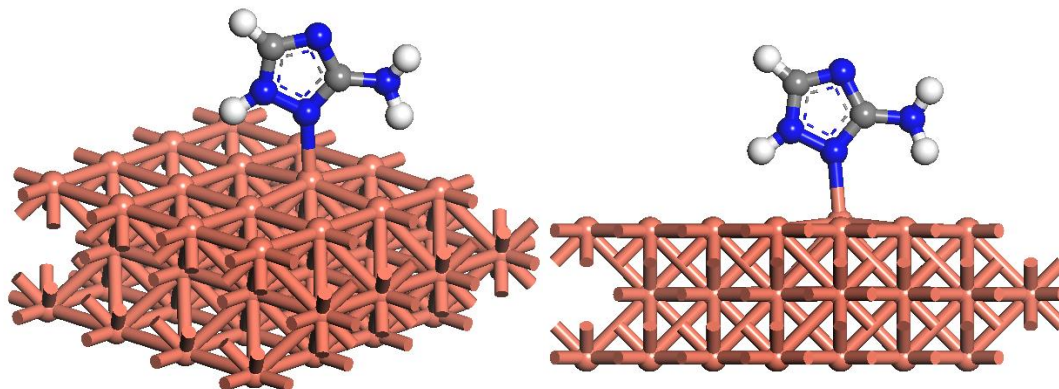


Figure 10. The adsorption model of ATA-Cu

4. CONCLUSIONS

(1) The $i_{ph, max}$ for the Cu electrode in borax buffer solution increased evidently on the negative potential scan, the larger the ATA concentration, the higher the cathodic photocurrent value and the better the inhibition effect. The photocurrent attains the maximum value when the concentration of ATA is $30 \text{ mg}\cdot\text{L}^{-1}$, indicating the best inhibition effect.

(2) ATA has good corrosion inhibition for copper in borax buffer solution. The inhibition efficiency attains the maximum value of 97.65% when the concentration of ATA is $30 \text{ mg}\cdot\text{L}^{-1}$.

(3) ATA can be spontaneously adsorbed on the surface of copper. Adsorption of the ATA is found to follow the Langmuir's adsorption isotherm, and the adsorption mechanism is typical of chemisorption.

(4) SERS confirmed that the adsorbed ATA molecules formed a complex with Cu^+ which prevented the formation of copper chloride complexes, CuCl_2^- .

(5) ATA would be adsorbed vertically through N3 atoms to the surface by the analysis of electrostatic potential and molecular orbital.

ACKNOWLEDGEMENTS

This work was financially supported by National Natural Science Foundation of China (No. 21673135) and Science and Technology Commission of Shanghai Municipality (No.17020500700).

References

1. B. P. Singh, S. Nayak, K. K. Nanda, B. K. Jena, S. Bhattacharjee and L. Besra, *Carbon*, 61 (2013) 47.
2. I. T. Vargas, M. A. Alsina, J. P. Pavissich, G. A. Jeria, P. A. Pastén, M. Walczak and G. E. Pizarro, *Bioelectrochemistry*, 97 (2014) 15.

3. B. Feier, I. Bajan, I. Fizesan, D. Floner, C. Cristea, F. Geneste and R. Sandulescu, *Int. J. Electrochem. Sci.*, 10 (2015) 121.
4. H. Tian, W. Li and B. Hou, *Int. J. Electrochem. Sci.*, 8 (2013) 8513.
5. B. A. Al Jahdaly and M. I. Awad, *Int. J. Electrochem. Sci.*, 11 (2016) 5473.
6. P. Majzlik, A. Strasky, V. Adam, M. Nemeč, L. Trnkova, J. Zehnalek, J. Hubalek, I. Provaznik and R. Kizek, *Int. J. Electrochem. Sci.*, 6 (2011) 2171.
7. G. Tansuğ, T. Tüken, E. S. Giray, G. Fındıkkıran, G. Sığırçık, O. Demirkol, and M. Erbil, *Corros. Sci.*, 84 (2014) 21.
8. H. Jie, Q. Xu, L. Wei, and Y. L. Min, *Corros. Sci.*, 102 (2015) 251.
9. W. Liu, Q. Xu, J. Han, X. Chen and Y. Min, *Corros. Sci.*, 110 (2016) 105.
10. M. Bertuola, C. A. Grillo and M. Fernández Lorenzo de Mele, *J. Hazard. Mater.*, 313 (2016) 262.
11. A. A. Abd-Elaal, I. Aiad, S. M. Shaban, S. M. Tawfik and A. Sayed, *J. Surfactants. Deterg.*, 17 (2014) 483.
12. M. Yadav, D. Behera, S. Kumar and R. R. Sinha, *Ind. Eng. Chem. Res.*, 52.19 (2013) 6318.
13. E. S. M. Sherif, R. M. Erasmus and J. D. Comins, *J. Colloid Interf. Sci.*, 311 (2007) 144.
14. E. S. M. Sherif, *Ind. Eng. Chem. Res.*, 52 (2013) 14507.
15. G. Žerjav, and I. Milošev, *Corros. Sci.*, 98 (2015) 180.
16. A. Zarrouk, B. Hammouti, A. Dafali and F. Bentiss, *Ind. Eng. Chem. Res.*, 52 (2013) 2560.
17. E. S. M. Sherif, *Int. J. Electrochem. Sci.*, 7 (2012) 1884.
18. M. Li, Q. Xu, J. Han, H. Yun and Y. Min, *Int. J. Electrochem. Sci.*, 10 (2015) 9028.
19. D. Gelman, D. Starosvetsky and Y. Ein-Eli. *Corros. Sci.*, 82 (2014) 271.
20. J. S. K. Arockiasamy and J. Irudayaraj, *Ceram. Int.*, 42 (2016) 6198.
21. C. Rahal, M. Masmoudi, R. Abdelhedi, R. Sabot, M. Jeannin and M. Bouaziz, *Electroanal. Chem.*, 769 (2016) 53.
22. W. Liu, W. Cao, X. Deng, Y. Min and Q. Xu, *Int. J. Electrochem. Sci.*, 10 (2015) 8858.
23. V. Mani, R. Devasenathipathy, S. M. Chen, S. F. Wang, P. Devi and Y. Tai, *Electrochim. Acta*, 176 (2015) 804.
24. S. H. Wang, X. W. Guo, S. U. N. Can, G. O. N. G. Jia, L. M. Peng and W. J. Ding, *T. Nonferr. Metal. So.*, 24 (2014) 3810.
25. M. B. Radovanović and M. M. Antonijević, *J. Adhes. Sci. Technol.*, 31 (2017) 369.
26. X. H. Zhang, Q. Q. Liao, K. B. Nie, L. L. Zhao, D. Yang, Z. W. Yue, H. H. Ge and Y. J. Li, *Corros. Sci.*, 93 (2015) 201.
27. P. Y. Chen, H. H. Yang, C. C. Huang, Y. H. Chen and Y. Shih, *Electrochim. Acta*, 161 (2015) 100.
28. X. Jin, Q. Xu, H. Liu, X. Yuan and Y. Xia, *Electrochim. Acta*, 136 (2014) 19.
29. X. Jin, Q. Xu, X. Yuan, L. Zhou, and Y. Xia, *Electrochim. Acta*, 114 (2013) 605.
30. X. Yuan, Q. J. Xu, C. Wang, X. Liu, H. Liu and Y. Xia, *J. Power Sources*, 279 (2015) 157.
31. B. M. Fernández-Pérez, J. A. González-Guzmán, S. González and R. M. Souto, *Int. J. Electrochem. Sci.*, 9 (2014) 2067.
32. S. B. Aoun, M. Bouklah, K. F. Khaled and B. Hammouti, *Int. J. Electrochem. Sci.*, 11 (2016) 7343.
33. P. O. Ameh and N. O. Eddy, *Res. Chem. Intermediat.*, 40 (2014) 2641.
34. H. Elmsellem, H. Nacer, F. Halaimia, A. Aouniti, I. Lakehal, A. Chetouani, S. S. Al-Deyab, I. Warad, R. Touzani and B. Hammouti, *Int. J. Electrochem. Sci.*, 9 (2014) 5328.
35. A. Singh, Y. Lin, E. E. Ebenso, W. Liu, D. Kuanhai, J. Pan and B. Huang, *Int. J. Electrochem. Sci.*, 9 (2014) 5585.
36. S. M. Tawfik, *J. Mol. Liq.* 207 (2015) 185.
37. Z. Z. Tasic, M. M. Antonijević, M. B. P. Mihajlović and M. B. Radovanovic, *J. Mol. Liq.*, 219 (2016) 463.
38. M. B. P. Mihajlović, M. B. Radovanović, Ž. Z. Tasić and M. M. Antonijević, *J. Mol. Liq.*, 225 (2017) 127.
39. Y. Zhang, S. Zhao, L. He and J. Zheng, *Trac-Trend. Anal. Chem.*, 90 (2017) 1.

40. Z. C. Zeng, S. C. Huang, D. Y. Wu, L. Y. Meng, M. H. Li, T. X. Huang, J. H. Zhong, X. Wang, Z. L. Yang and B. Ren, *J. Am. Chem. Soc.*, 137 (2015) 11928.
41. R. Caputo, *J. Electron. Mater.*, 45 (2016) 999.
42. W. Studziński, A. Gackowska, M. Przybyłek and J. Gaca, *Environ. Sci. Pollut. R.*, (24) (2017) 4049.
43. F. A. Soto and P. B. Balbuena, *Electrochim. Acta*, 220 (2016) 312.
44. S. Sun, Y. Geng, L. Tian, S. Chen, Y. Yan and S. Hu, *Corros. Sci.*, 63 (2012) 140.
45. A. Kosari, M. H. Moayed, A. Davoodi, R. Parvizi, M. Momeni, H. Eshghi and H. Moradi, *Corros. Sci.*, 78 (2014) 138.

© 2017 The Authors. Published by ESG (www.electrochemsci.org). This article is an open access article distributed under the terms and conditions of the Creative Commons Attribution license (<http://creativecommons.org/licenses/by/4.0/>).